Regarding the Line-of-Sight Baryonic Acoustic Feature in the Sloan Digital Sky Survey and Baryon Oscillation Spectroscopic Survey Luminous Red Galaxy Samples

Eyal A. Kazin,[a1] **Michael R. Blanton,**[a] **Román Scoccimarro,**[a]
Cameron K. McBride,[b] **Andreas A. Berlind**[b]
[a] *Center for Cosmology and Particle Physics, New York University, 4 Washington Pl., New York, NY 10003, USA*
[b] *Department of Physics and Astronomy, Vanderbilt University, 1807 Station B, Nashville, TN 37235, USA*

ABSTRACT

We analyze the line-of-sight baryonic acoustic feature in the two-point correlation function ξ of the Sloan Digital Sky Survey (SDSS) luminous red galaxy (LRG) sample ($0.16 < z < 0.47$). By defining a narrow line-of-sight region, $r_p < 5.5\,h^{-1}$Mpc, where r_p is the transverse separation component, we measure a strong excess of clustering at $\sim 110\,h^{-1}$Mpc, as previously reported in the literature. We also test these results in an alternative coordinate system, by defining the line-of-sight as $\theta < 3^\circ$, where θ is the opening angle. This clustering excess appears much stronger than the feature in the better-measured monopole. A fiducial ΛCDM non-linear model in redshift-space predicts a much weaker signature. We use realistic mock catalogs to model the expected signal and noise. We find that the line-of-sight measurements can be explained well by our mocks as well as by a featureless $\xi = 0$. We conclude that there is no convincing evidence that the strong clustering measurement is the line-of-sight baryonic acoustic feature. We also evaluate how detectable such a signal would be in the upcoming Baryon Oscillation Spectroscopic Survey LRG volume (BOSS). Mock LRG catalogs ($z < 0.6$) suggest that: (*i*) the narrow line-of-sight cylinder and cone defined above probably will not reveal a detectable acoustic feature in BOSS; (*ii*) a clustering measurement as high as that in the current sample can be ruled out (or confirmed) at a high confidence level using a BOSS-sized data set; and (*iii*) an analysis with wider angular cuts, which provide better signal-to-noise ratios, can nevertheless be used to compare line-of-sight and transverse distances, and thereby constrain the expansion rate $H(z)$ and diameter distance $D_{\rm A}(z)$.

Subject headings: **cosmology: observation - distance scale - galaxies: elliptical and lenticular, cD - large scale structure of universe**

Submitted to The Astrophysical Journal
April 12th 2010

[1] eyalkazin@gmail.com

1. Introduction

The baryonic acoustic feature serves as an important tool for our understanding of the evolution of the universe (Peebles & Yu 1970). Orig-

inating from plasma sound-wave residuals that came to a near stop at the end of the baryon drag epoch ($z_d \sim 1010$), it has the potential to serve as a cosmic *standard ruler*, which, in turn, can help us measure the expansion of the universe (Hubble & Humason 1931, Blake & Glazebrook 2003, Seo & Eisenstein 2003, Hu & Haiman 2003, Linder 2003, Glazebrook & Blake 2005).

In galaxy clustering measurements, this feature is a peak of over-density at separations of $s \sim 100\,h^{-1}$Mpc in the two point correlation function ξ, which results in an oscillatory feature in the power spectrum P(k).

Eisenstein et al. (2005) were the first to detect this feature, using the clustering of $\sim 44,000$ luminous red galaxies (LRGs) from the Sloan Digital Sky Survey (SDSS; York et al. 2000). Their measurement of the angle-averaged ξ, which is commonly referred to as the *monopole*, has the power to constrain a combination of the Hubble expansion rate $H(z)$ and the angular diameter distance $D_{\rm A}(z)$.

To measure H and $D_{\rm A}$ separately, one would like to probe the baryonic acoustic feature independently along the line-of-sight and transverse directions (Matsubara 2004). Measurements of these potentially promising methods are currently strongly compromised by shot noise and sample variance limitations, due the large scale nature of the feature. For this reason, most studies have focused on measuring and analyzing the baryonic acoustic feature in the angle averaged ξ (Martinez et al. 2008, Cabré & Gaztañaga 2009, Labini et al. 2009, Sanchez et al. 2009, Kazin et al. 2010), P(k) (Cole et al. 2005, Tegmark et al. 2006, Hütsi 2006, Percival et al. 2007, Percival et al. 2009, Reid et al. 2009) and the projected two-point function of photo-z samples (Padmanabhan et al. 2007, Blake et al. 2007) in the SDSS and and Two Degree Field Galaxy Redshift Survey (Colless et al. 2003) galaxy samples.

Gaztañaga, Cabré, & Hui (2009) (hereafter referred to as GCH), however, claim to have measured the line-of-sight baryonic acoustic feature. Using $\sim 77,000$ LRGs from the SDSS Data Release 6 (DR6, Adelman-McCarthy et al. 2008) and $\sim 100,000$ from DR7 (Abazajian et al. 2009) they report a significant detection of a feature at $\pi \sim 110\,h^{-1}$Mpc in the line-of-sight direction, within a projected distance of $r_p < 5.5\,h^{-1}$Mpc.

The clustering excess they focus on appears much stronger than expected from the baryonic acoustic feature according to the concordance ΛCDM model. The galaxies are observed in *redshift-space*, as opposed to real-comoving-space. In redshift-space (z-space) the line-of-sight peak in the non-linear correlation function is expected to smear heavily due to velocity dispersion. Furthermore, the whole correlation function should appear negative due to the strong squashing effect (Kaiser 1987) at scales $s > 50\,h^{-1}$Mpc in the line-of-sight direction.

These predictions suggest that if the sharp strong positive measurement obtained by GCH is the real feature, it would require a physical explanation.

Magnification bias has been proposed to increase clustering at the feature scales. This effect results from gravitational lensing modifying the spacial distribution of high redshift objects (Turner et al. 1984, Hui et al. 2007 and references within). Yoo & Miralda-Escudé (2009) and GCH examine this effect for the redshift-space ξ at $z = 0.35$. Both studies agree that the magnification effect is anisotropic having the strongest impact on the line-of-sight. GCH show that a model with magnification performs slightly better than without (2σ level). We do not include an analysis of magnification bias in this study, but show that the line-of-sight clustering does agree well with a fiducial ΛCDM model without a magnification bias.

In particular, Miralda-Escude (2009) argues, using pair-count statistics (based on data analyzed by GCH), that the clustering excess is not significant, and should not be regarded as a detection of the baryonic acoustic feature. We concur with that conclusion here.

The purpose of this study is to revisit the line-of-sight clustering signal in the SDSS LRG sample, examine its reliability and predict the signal

and its uncertainties obtainable in the much larger volume and denser Baryonic Oscillation Spectroscopic Survey sample (BOSS; Schlegel et al. 2009).

We measure the line-of-sight clustering ξ at sfcales of $40 - 200\,h^{-1}$Mpc , finding results similar to that obtained by GCH. We predict z-space (as well as real-space) signals and uncertainties for SDSS-sized volumes, by using very realistic light-coned mock galaxy catalogs which are based on fiducial ΛCDM models.

In §2 we briefly explain the data and mock catalogs used for analysis. In §3 we present the anisotropic ξ clustering and the coordinate systems used throughout the study. In §4 we analyze the line-of-sight clustering of DR7-Sub, and in §5 we perform a similar analysis on the larger DR7-Full, and directly compare results with GCH. We examine the significance of the strong line-of-sight clustering signal in §6 by applying a Jeffreys scale to compare model fits to data performed here and in GCH. In §7 we predict the line-of-sight measurement expected from the BOSS sample, along with a detailed comparison of the signal-to-noise ratios of the three volumes discussed here. In §8 we vary the definition of line-of-sight to wider wedges, to show that BOSS may be used to disentangle $H(z)$ and $D_{\rm A}(z)$.

In the following, all calculations assume a flat ΛCDM model. When converting data redshifts to comoving distances, we assume a present day matter density Ω_{M0}=0.25, and define $H_0 = 100h$ km s^{-1} Mpc^{-1}.

2. Data and Methods of Analysis

Here we briefly present the SDSS LRGs as well as mock realizations used for testing systematics and measurement uncertainties. In depth descriptions of the data and mock catalogs used here, as well of methods of analysis, are given in our previous study of the monopole (Kazin et al. 2010).

In Table 1 we summarize the different volumes discussed in this study.

2.1. SDSS-II LRGs

We use the LRG sample from the final release (DR7) of the SDSS.

In what follows, DR7-Full is defined as the full range of the SDSS LRG sample ($0.16 < z < 0.47$). We also define a subsample DR7-Sub, which focuses on the quasi-volume-limited region ($z < 0.36$; see Figures 1, 2 in Kazin et al. 2010, in which the latter is called there DR7-Dim[2]).

We calculate ξ by using the Landy & Szalay (1993) estimator, which requires the use of a catalog of random points. For DR7-Full we use 15 random points for each LRG, and for DR7-Sub we use 50.

The LRG data set and random points used here are accessible on the World Wide Web.[3]

2.2. Mock LRGs

To predict ξ and its uncertainties in three different volumes (DR7-Sub, DR7-Full and BOSS), we make use of mock realizations for each volume. For DR7-Sub we use mocks provided by the LasDamas collaboration (McBride et al., in preparation), and for the other two samples we use mocks generated by the Horizon Run (Kim et al. 2009).

The LasDamas simulations use a cosmology of $[\Omega_{M0}, \Omega_{b0}, n_s, h, \sigma_8]$=[0.25,0.04,1,0.7,0.8] and the Horizon Run uses [0.26,0.044,0.96,0.72,0.8], where Ω_{b0} is the present baryonic density and n_s is the spectral index. Both these cosmologies are well motivated by constraints obtained by WMAP 5-year measurements of temperature fluctuations in the cosmic microwave background (Komatsu et al. 2009).

The LasDamas collaboration provides very realistic LRG mock catalogs[4] by placing galaxies inside dark matter halos using a Halo Occupation Distribution (HOD; Berlind & Weinberg 2002). HOD parameters were chosen to reproduce the

[2] DR7-Sub (DR7-Dim) is not a dimmer sample of galaxies than DR7-Full, but a subsample limited by $z < 0.36$. The term "dim" was used in our previous study to distinguish from a brighter overlapping subsample of DR7-Full.

[3] http://cosmo.nyu.edu/∼eak306/SDSS-LRG.html

[4] http://lss.phy.vanderbilt.edu/lasdamas/

observed number density as well as the projected two-point correlation function $w_p(r_p)$ of galaxies at separations $0.3 < r_p < 30\,h^{-1}$Mpc, far below the scales considered here, and independent of the line-of-sight clustering. We use 160 LRG mock light-cone z-space realizations that have a matching radial selection function and angular mask to that of DR7-Sub.

For reasons explained in §4, we analyze all volumes both in $z-$space and real-space. The LasDamas real-comoving-space catalog is similar to the redshift-space catalog in all aspects, except the shift in z due to peculiar velocities. Another small difference is that we do not mock the observed comoving density $n(z)$ by diluting the original mock sample, but use the whole real-space catalog. In Appendix A.2 and Figure 13 of Kazin et al. (2010) we discuss the negligible differences between a sample with the observed $n(z)$ to that originally provided by LasDamas. For both redshift and real-space we use a ratio of ~ 50 random points for each mock data.

The Horizon Run[5] provides a catalog of 32 BOSS volume realizations of mock LRGs with a higher number density than DR7, as expected in BOSS ($n \sim 3 \cdot 10^{-4} h^3$ Mpc^{-3} in BOSS, which drops quickly after $z \sim 0.6$, vs. $\sim 0.9 \cdot 10^{-4} h^3$ Mpc^{-3} in DR7-Sub). LRG positions are determined by identifying physically self-bound dark matter sub-halos that are not tidally disrupted by larger structures. Our only manipulations of the real-space catalogs are to divide each of their eight full sky samples into four quadrants each to map real-space into redshift space, and to limit the samples to the expected volume-limited region of the BOSS LRGs ($0.16 < z < 0.6$). This results in $8 \times 4 = 32$ BOSS mock realizations. For the BOSS volume analysis we use ~ 2 random points per mock data in z-space and real-space.

For our DR7-Full volume analysis we limit each realization to the range $0.16 < z < 0.47$. DR7-Full has a flux-limited region ($0.36 < z < 0.47$; see Figure 2 in Kazin et al. 2010), meaning that as z increases the sample is more biased towards the more luminous LRGs. This also affects the number counts of galaxies, meaning an increase in shot noise.

We attempt to take these two effects into account by subsampling the original Horizon Run catalog to fit the observed selection function. The Horizon Run team provides halo masses, which we use in Equation 3 from Park & Kim (2007) to subsample. In each realization we limit ourselves to 7908 deg^2 to match the SDSS volume of DR7-Full. The number count of the mock halos is similar to that of the LRGs. For the DR7-Full volume analysis we use ~ 10 random points per mock data.

3. Results: Anisotropic Clustering ξ(2D)

In Figure 1 we show the anisotropic ξ of DR7-Full. Redshift distortions due to peculiar velocities are apparent. On small scales the velocity-dispersion effect dominates line-of-sight clustering (Jackson 1972), and on large scales gravitational infall causes a squashing effect (Kaiser 1987) that distorts the contours towards smaller scales along the line-of-sight.

The top panel shows $\xi(r_p, \pi)$ in the standard coordinates: π is the line-of-sight component of pair separation s; r_p is the transverse component. Redshift distortions in this logarithmic contour plot appear as deviations from circles. The effect of velocity dispersion is clearly seen as the feature at small r_p. On larger π scales the squashing effect is evident. Two notable features are the "negative sea" on the line-of-sight (also shown by Cabré & Gaztañaga 2009) and the baryonic acoustic ridge (Okumura et al. 2008, GCH).

The bottom panel shows the same information in a different coordinate system. We define s as the separation length in redshift-space:

$$s = \sqrt{\pi^2 + r_p^2}, \tag{1}$$

and θ is the polar angle from the line-of-sight direction, i.e, $\cos(\theta) = \pi/s$. In these coordinates, redshift distortions appear as deviations from horizontal lines. In Kazin et al. (in preparation) we give a full description of our angular analysis methods when examining the distortions on scales

[5] http://astro.kias.re.kr/Horizon-Run/

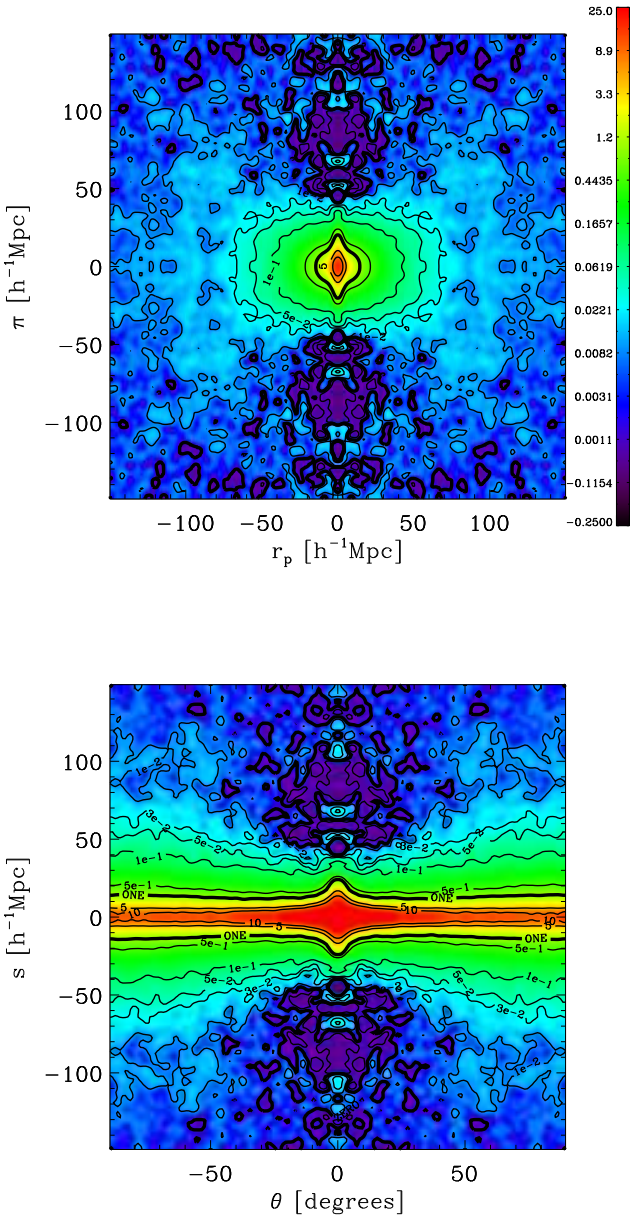

Fig. 1.— DR7-Full Anisotropic $\xi(\vec{s})$. Top panel shows the $\pi - r_p$ plane; in these coordinates redshift distortions are deviations from circles; Bottom panel shows the $s - \theta$ plane; redshift distortions are deviations from horizontal lines. $\theta = 0^\circ$ is the line-of-sight direction. The color coding is the same for both, where the strongest signal is red and the purple is a negative region. Contour lines indicate values of 10, 5, 1 (thick), 0.5, 0.1, 0.05, 0.03, 0.01, 0 (thick), and −0.01. For the purposes of these plots, we have smoothed the correlation function using a Gaussian filter with $\sigma = 5\,h^{-1}$Mpc in distance, and with $\sigma = 3^\circ$ in angle.

$s < 80\,h^{-1}$Mpc. Briefly, when counting pairs, we define the line-of-sight direction ($\theta = 0^\circ$) as the vector that bisects the pair separation vector, and all four quadrants are binned into one. We mirror this quadrant symmetrically for presentation purposes. For clarity, these plots have been smoothed using a Gaussian filter with $\sigma = 5\,h^{-1}$Mpc in r_p, π and s (both panels) and $\sigma = 3^\circ$ in θ (bottom panel).

We turn our focus to the region containing the line-of-sight baryonic acoustic feature reported by GCH. In Figure 1 this region appears as the bright positive spot (cyan) at $s(\theta \sim 0^\circ) = 100\,h^{-1}$Mpc in the bottom panel (or alternatively at $\pi(r_p \sim 0\,h^{-1}\text{Mpc}) \sim 100\,h^{-1}$Mpc in the top). These plots show a sharp bright clustering excess with $\xi > 0.05$ at larger scales than that of the negative sea (purple).

These plots can be misleading, due to the smoothing, so we now focus on one dimensional angular cuts.

Before performing a direct comparison with results obtained by GCH on the full sample ($0.16 < z < 0.47$; §5), which is flux limited, in the next section we focus on a quasi-volume limited sample ($0.16 < z < 0.36$).

4. Results: DR7-Sub ($0.16 < z < 0.36$) Line-of-Sight Clustering

In their Figure 15, GCH show strong line-of-sight clustering measurements where we expect to detect the baryonic acoustic feature. Here we perform a similar procedure to reproduce their results. Two main differences are: (1) They examine $0.15 < z < 0.30$, where we probe $0.16 < z < 0.36$; (2) We analyze here both the s-θ plane, and $\pi - r_\mathrm{p}$.

In this section, when analyzing the $s - \theta$ plane, we define *line-of-sight clustering* as $\langle \xi(s, 0^\circ < \theta < \theta_\mathrm{max}) \rangle$, where

$$\langle \xi(s, \theta_\mathrm{range}) \rangle = \int_{\theta_\mathrm{min}}^{\theta_\mathrm{max}} \xi(s, \theta) \sin(\theta) d\theta \qquad (2)$$

In practice we calculate $\langle \xi(s, \theta_\mathrm{range}) \rangle$ by counting all pairs within the bin of dimensions $\Delta\theta$ and Δs.

When analyzing the $\pi - r_{\rm p}$ plane we define line-of-sight clustering, as in GCH, as $\left\langle \xi(\pi, r_p^{\rm min} < r_p < r_p^{\rm max}) \right\rangle$. In practice this means that we count all pairs within these bins, and apply our ξ estimator. In order to avoid fiber collision effects, GCH limit themselves to r_p region $[0.5, 5.5]\,h^{-1}$Mpc. We test effects of fiber collisions by comparing data results with and without fiber collision corrections in weighting when counting galaxy pairs, as well as with and without region $r_p < 0.5\,h^{-1}$Mpc and find no significant difference in results (see Kazin et al. 2010 for details on fiber collision effects on the correlation function monopole)

Here we use $\theta_{max} = 3^\circ$, corresponding to $0.5 < r_p < 5.5\,h^{-1}$Mpc at $s \sim 100\,h^{-1}$Mpc. This choice means that one expects similar line-of-sight clustering measurements and uncertainties at scales of the baryonic acoustic feature. In §7 we discuss. similarities and differences between these coordinate systems.

Figure 2 displays our line-of-sight results in both coordinate systems. In the top panels of both plots, DR7-Sub line-of-sight clustering results are shown by the black diamonds.

As in Figure 1, the region between 50 and $100\,h^{-1}$Mpc is mostly negative.

At scales of $\sim 110\,h^{-1}$Mpc (adjacent to the red upward arrow, which indicates the line-of-sight peak position according to GCH) we see a strong line-of-sight clustering excess in DR7-Sub, which is much stronger than the baryonic acoustic feature in the monopole (crosses; Kazin et al. 2010). Notice the agreement, as expected, between the high excess at scale $108.9\,h^{-1}$Mpc in both choices of coordinate systems.

In the top panels of Figure 2 we show the expected redshift line-of-sight result (solid red line with uncertainty bars on the mean of 160 realizations), as well as the 1σ (68% C.L; bright gray band) and 2σ (95% C.L; dark gray) regions for a single DR7-Sub sample. The blue dotted lines are not one realization in particular, but the outermost values of all mocks. The gray bands show the large scatter around the expected mean.

The expected (mock mean) line-of-sight baryonic acoustic feature is not obvious, but appears suppressed and smeared. This lack of clear detection might result from the limited statistical power available even from 160 mock catalogs.

Redshift distortions also weaken the signal. To evaluate their importance, we examine the line-of-sight ξ obtained from the real-space LasDamas mocks, which are not affected by the peculiar velocities.

In the bottom panels of Figure 2, we compare the expected line-of-sight signal in the LasDamas real-space (thin green solid line) and redshift-space (thick red solid line; same as top panel) to the monopoles to which they each contribute (thin green dashed and thick red dotted, respectively). The data monopole is the same as in the top panel.

The real-space line-of-sight mock mean traces the monopole very well until $\sim 30\,h^{-1}$Mpc (not shown here) and continues with a similar trend, though with considerable noise. Notice that at $\sim 110\,h^{-1}$Mpc the $\pi - r_p$ system (top panel) and $s - \theta$ (bottom) both show signals appear similar to the monopole, but with more noise. There is an indication of a peak, but it is not obvious.

We remind the reader that the uncertainty bars on the line-of-sight mock signals (solid green and red) are for the mock mean (of 160), not one for one DR7-Sub volume. This means that, even given a volume 100 times that of the DR7-Sub sample, a line-of-sight peak (as defined here) would not be obvious in real-space and in redshift-space it would be totally washed out. In §8 we show that by using wider line-of-sight wedges the signal-to-noise increases, yielding an apparent feature.

As another consistency check, we perform the same line-of-sight test on a mock catalog with larger volume and higher density (Horizon Run; $z < 0.6$; see §2.2). Using 32 realizations of real-space catalogs, we obtain a mock mean of $\langle \xi(s, 0^\circ < \theta < 3^\circ) \rangle$ that mimics the monopole with baryonic acoustic feature peak positions in fair agreement.

We also estimate uncertainties with jackknife subsampling of the data, using 24 equal area subsamples (as used in Kazin et al. 2010). The jackknife uncertainties are similar to those determined

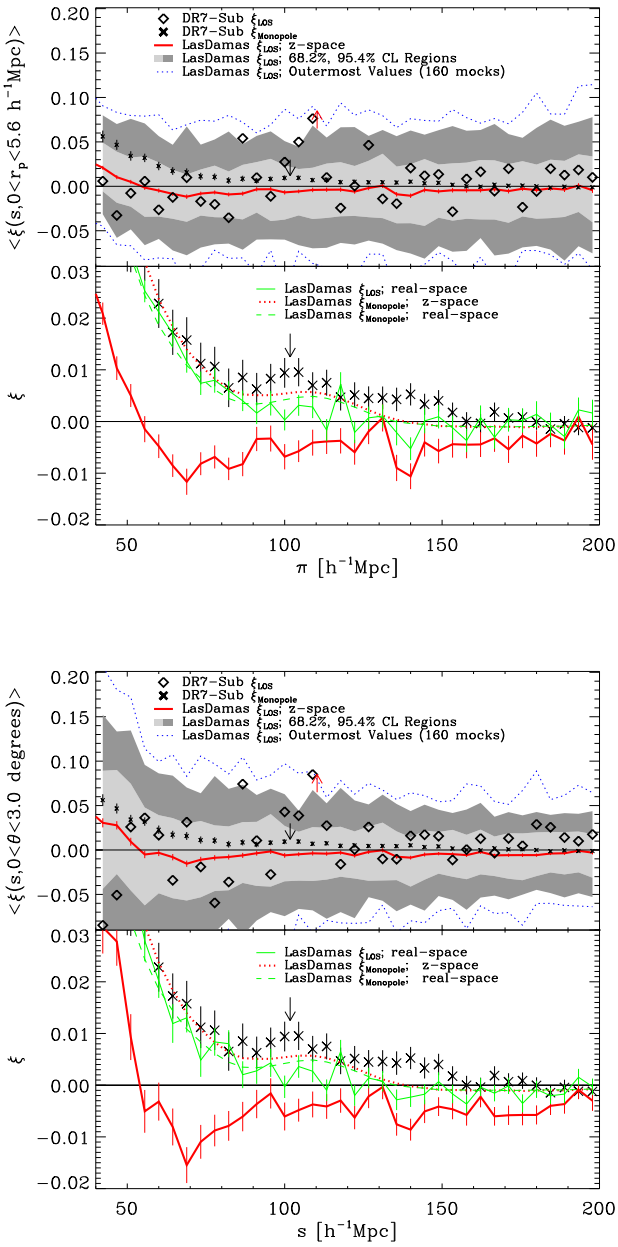

Fig. 2.— DR7-Sub line-of-sight ξ. Both plots contain same information, but in different coordinate systems. On the top $\xi_{\rm LOS}(\pi, r_{\rm p} < 5.6\,h^{-1}{\rm Mpc})$, and on the bottom $\xi_{\rm LOS}(s, \theta < 3^{\circ})$, as defined in the text. The monopoles are the same for both. Top Panels: Diamonds are the SDSS DR7-Sub LOS result. The crosses are the monopole $\xi_{\rm Monopole}$ for comparison. The solid red line is the LasDamas mock mean line-of-sight correlation function (with uncertainties indicating variance of the mock mean). The bright and dark gray bands indicate the 68.2% and 95.4% CL regions, respectively, for a given DR7-Sub volume. The blue dotted lines are the outer-most values at each scale for all 160 mocks. The black downward arrow indicates the baryonic acoustic feature peak location in the monopole. The red arrow upward is where GCH claim to detect a "peak position" in the line-of-sight direction. Bottom Panel: testing LOS real and z-space vs monopole. The crosses and the thick solid lines are the same as before. The red dotted line is the mock monopole in redshift-space, and the green dashed line is the mock monopole in real-space. The thin solid green line is mean real-space line-of-sight signal from all the mocks. The black downward arrow again shows the monopole peak position according to Kazin et al. (2010).

from the mock catalogs (Figure 5).

To test the consistency of the DR7-Sub measurement with the mock-mean value we perform a χ^2 fit, where the (noisy but invertible) covariance matrix is constructed from all 160 mock realizations (data point uncertainties are correlated). Examining the range 40–140 h^{-1}Mpc we obtain $\chi^2 = 30.6$ (23.2) for 23 (20) degrees of freedom (dof) when defining line-of-sight as $r_p < 5.5\,h^{-1}$Mpc, and $\chi^2 = 31.7$ (24.8) when using $\theta < 3^\circ$. A $\xi = 0$ model yields $\chi^2 = 26.5$ (23.2) and 27.0 (29.0). For these measurements we use binning $\Delta\pi = 4.4$ (5.0) h^{-1}Mpc and $\Delta s = 4.4$ (5.0) h^{-1}Mpc, respectively.

These results show that when using the smaller binning of $4.4\,h^{-1}$Mpc, all these tests indicate a $\sim 1\sigma - 1.5\sigma$ agreement between the data and the expected result, and even agree even better with a null hypothesis. Widening the bins ($5.0\,h^{-1}$Mpc) yields even better agreements.

When restricting the test around the expected baryonic acoustic feature at $100 - 125\,h^{-1}$Mpc we obtain $\chi^2 = 11.2$ (13.6) for 6 (5) dof, and $\chi^2 = 11.3$ (13.4) for r_p and θ line-of-sight definition, respectively. A $\xi = 0$ model yields $\chi^2 = 9.9$ (12.1) and 10.1 (11.75).

When widening the bins ($5.0\,h^{-1}$Mpc), the null hypothesis yields better results than the observation, though the data agrees only at a $\sim 2\sigma$ level.

These tests show that the line-of-sight observation is in good agreement with a fiducial ΛCDM model.

Next section we perform the same analysis on DR7-Full, which has a much larger volume. We also compare results directly with GCH.

5. Results: DR7-Full ($0.16 < z < 0.47$) Line-of-Sight Clustering

In the top panel of Figure 3 we show a direct comparison between our DR7-Full line-of-sight clustering $\xi_{\rm LOS}$ results (black diamonds) to those in Table 1 of GCH and their Figure 15 (purple triangles; DR6). The 1σ uncertainties on our data are explained below. We omit uncertainties of GCH to avoid cluttering, but show in Figure 5 that our uncertainties are similar to theirs on these scales.

As expected, the measurement is very noisy. Our results are similar to those obtained by GCH, in two ways. First, we both measure the negative region between $50 - 95\,h^{-1}$Mpc, and second, we each measure a *very* high value that happens to be where one expects the acoustic feature to be. This strong excess at $\pi \sim 110\,h^{-1}$Mpc appears five times stronger than that obtained in the much higher signal-to-noise ratio monopole (crosses; Kazin et al. 2010).

In §2.2 we explain the technical details of diluting the original Horizon Run mocks (which were originally designed for BOSS volume and density), to the properties of DR7-Full. The resulting expected z-space monopole is shown as the red dotted line in the bottom panel of Figure 3. The agreement with the data around the baryonic acoustic feature seems good. However, we do notice a $\sim$ 10% bias difference ($\sqrt{\xi_{\rm mocks}/\xi_{\rm SDSS}}$) at smaller scales. This might indicate that we have excluded a few more low mass halos than we should have, since clustering is known correlate with mass (Zehavi et al. 2005). We doubt that this mismatch will affect our line-of-sight analysis around the baryonic acoustic feature. In the previous section we obtained similar conclusions to those presented here when using very realistic mocks provided by LasDamas, that are fit to data on low scales. In the bottom panel of Figure 5 we also show excellent agreement between our uncertainty measurements and those obtained by GCH.

The predicted line-of-sight correlation function in redshift-space is shown in both panels of Figure 3 as the solid thick red lines. The bottom panel is a zoomed-in version of the top. The uncertainty bars indicate the uncertainty in the mock mean given 32 realizations. In the top panel of Figure 3, the gray band indicates the 68.2% confidence level (CL) region for a single volume, and the blue dotted lines are the outermost values of all mocks (not one in particular).

We see that the expected line-of-sight correlation function has a negative valley around 55–$100\,h^{-1}$Mpc. The signal increases towards the

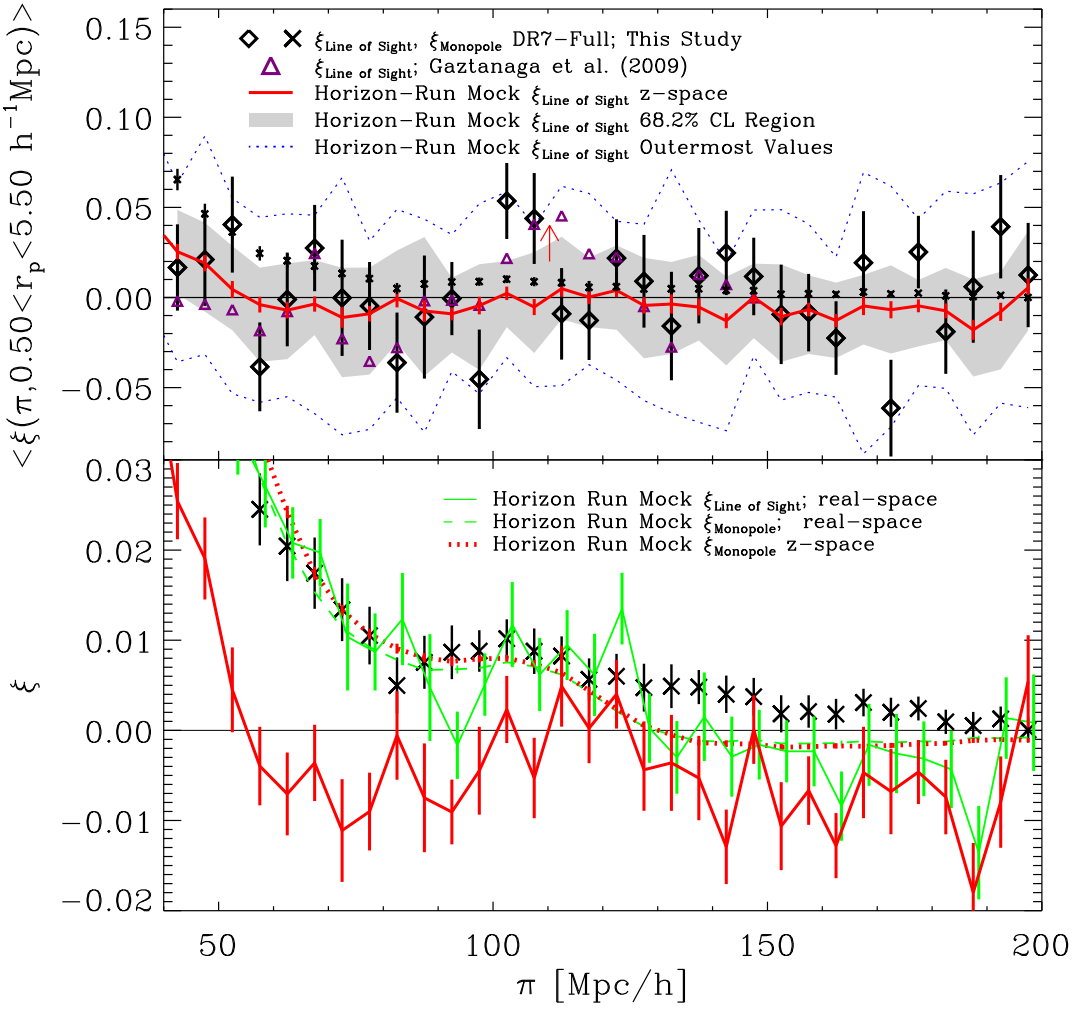

Fig. 3.— DR7-Full line-of-sight $\xi(\pi, r_p < 5.6\,h^{-1}\text{Mpc})$. The legend here is the same as in Figure 2 with a few differences- mock results are based on 32 Horizon Run mocks, we add results from GCH (purple triangles) for direct comparison

baryonic acoustic feature area and decreases on larger scales.

Comparing these predictions to observation, we see that the very strong measurement at $\pi \sim 100\,h^{-1}$Mpc, although unlikely, is still acceptable according to the mock realizations.

We note that, although our measurements are very similar, we do not obtain the exact same results as GCH. Differences might result from any combination of systematics in analysis. For example, our methods of weighting galaxies may slightly differ when counting pairs, or perhaps it may be due to the differences in the samples (we use $\sim 105,000$ LRGs where they use $\sim 77,000$). When comparing the much more stable monopole we obtain similar results to theirs. As for the anisotropic ξ we find that we obtain a similar normalized quadrupole $Q(s)$ to that published in Cabré & Gaztañaga (2009).

Our line-of-sight ξ results, as well as covariance matrices, may be obtained on the World Wide Web.[6]

6. Interpretation of Data Results

In the previous section we show that our measurements are very similar to those previously obtained by GCH and in see Figure 5 we show agreement in uncertainty estimates. These agreements show that the results are not sensitive to minor systematic differences (selection of LRGs, weighting algorithms, etc.). We do, however, disagree on the interpretation of the results, as we now clarify. The main distinction between the two interpretations is that we do not agree on the importance of a null $\xi = 0$ test. They claim that it is *"only slightly disfavored compared to the best-fit model"*. Here we compare the null test to physical models and conclude that the $\xi = 0$ is a good fit to the data, and physical models do not perform significantly better. This means that the line-of-sight data *alone* is too noisy to infer the presence of a peak.

GCH argue for a significant detection of the line-of-sight baryonic acoustic feature based on χ^2 fits to the data (see their Figures 13 and 15). Here we investigate the significance of their results compared to ours.

In Table 2 we summarize the χ^2 results they and we obtain with various models on similar data sets. We analyze DR7-Sub and DR7-Full, while GCH investigate the full DR6 as well as a smaller volume ($0.15 < z < 0.30$). In all cases the line-of-sight $\xi(\pi, r_p < 5.5\,h^{-1}\text{Mpc})$ is investigated at scales of $40 < \pi < 140\,h^{-1}$Mpc with bin widths of $\Delta\pi = 5\,h^{-1}$Mpc ($N = 20$ bins).

The models that GCH investigate are:

1. BAO: best fit ΛCDM based line-of-sight model based on $k = 5$ parameters.
2. BAO+mag: same as BAO including lensing magnification effect ($k = 6$).
3. No BAO: a ΛCDM model based on a featureless P ($k = 5$).
4. $\xi = 0$: Null test ($k = 0$).

We investigate two fiducial flat ΛCDM models based on our mocks (LasDamas, Horizon Run). These models are very similar ($\Omega_{M0} = 0.25, 0.26$, respectively). As we do not vary the cosmology in our estimates, here we use $k = 0$. Both use N-body simulations that produce very realistic mock LRG catalogs. As described in §2.2, the mocks take many observational effects into account. Assuming the correctness of ΛCDM, this procedure yields very reliable uncertainties (C_{ij}), as well as non-linear fiducial models. The models used by GCH are analytical (giving them the advantage of probing many cosmological models), but they do not account for effects of the survey mask in their modeling or in their C_{ij}.

We also investigate the $\xi = 0$ model, which is, of course, not a physical one. It is, however, an interesting straw-man model in the context of claiming a detection.

We test our models on both our data, and those in Table 1 of GCH (with our own covariance matrices).

[6] http://cosmo.nyu.edu/∼eak306/BAF.html

Examining the reduced χ^2 column ($\chi^2/(N-k)$) in Table 2 , we conclude that the data agrees fairly well with all the models tested. We see this in the *Prob* column which indicates the probability of a random variable from a χ^2 distribution with $N-k$ degrees of freedom to have a value larger than that in the χ^2 column. Notice that all models range betwen $4.5\% - 96\%$. In other words, all models fit the data at 2σ or better. This procedure tests each model independently, but to compare between them is more complicated.

There are various ways to compare models and determine significance of difference. Here we present a few common tests used in the literature (Liddle 2009 and references within).

The Jeffreys scale uses a value called the "Evidence" E, which is the average likelihood of the parameters averaged over the parameter prior. The difference of $\ln E$ may be used to describe how much better one model agrees with data from another. For example, in order for one model to perform significantly better than another, $\Delta \ln E$ should be larger than unity. Other useful divisions in significance is for values 2.5 (posterior odds of $12:1$) and 5 ($148:1$; see caption of Table 2).

We approximate E by using the Bayesian information criterion (BIC; Schwarz 1978) defined as

$$-\ln(E) \sim \mathrm{BIC} = -2\ln(L_{max}) + k\ln(N), \quad (3)$$

where k is the number of parameters, N is the number of data points. Assuming the liklihood L is Gaussian $-2ln(L_{max}) = \chi^2_{min}$. Using this criterion, we prefer models that yield a lower BIC result. A similar technique is the Akaike Information Criterion (AIC; Akaike 1974) defined by replacing $k\ln N$ with $2k$. Both these criteria are summarized in Table 2 in separate columns.

Applying BIC and AIC to the GCH results, the "No BAO" model is clearly disfavored in respect with the other models. This result does not mean, however, that the data reveal a significant line-of-sight baryonic acoustic feature. One way to look at this is to realize that $\xi = 0$ is a good fit. Below we elaborate on this point.

For completeness we mention that the χ^2 for the physical models posted in GCH might be misestimated for the purpose of comparing them to each other. When fitting models to data they use a Gaussian prior likelihood indicated in their Section 3.8.2. This prior should be taken into account when calculating the full χ^2. This means that an additional term $\chi^2_{\rm prior} = \sum_{i=0}^{N_{\rm prior}} (\gamma_i - \gamma_i^{\rm prior})^2/\sigma^2_{\gamma_i}$, where γ_i is the $i^{\rm th}$ parameter, should be added. They use $N_{\rm prior} = 4$ parameters as priors: [Ω_b, Ω_{M0}, $b\sigma_8$, β], where β is the Kaiser squashing parameter, and b is the linear bias factor relating matter and LRG over-densities. Through private communication with the authors we learn that their best fit values for the BAO+mag model are $[0.049,\ 0.240, 1.73, 0.39]$ This yields $\chi^2_{\rm prior} = 9.4$ which should be added to their stated $\chi^2 = 8$, and correcting the number of data points from $N = 20$ to 24 (one additional "data point" for each prior). They claim that they obtain similar parameter values (γ_i) for the other physical models, so when comparing between them this term should approximately cancel out. It is not clear, however, the correct manner to incorporate this correction utilizing BIC and AIC when comparing with $\xi = 0$ and our mock models which do not use prior likelihoods. For simplicity we quote in Table 2 values published by GCH.

So far we have used a rigid definition of number of parameters k. A thorough analysis would investigate the relative influence of each parameter on the model. This could be done by investigating the full parameter space, which is out of the scope of this study. To attempt to minimize effect of free parameters, we asked the authors of GCH, through private communication, for results using the minimum number of free parameters. Setting all parameters to the prior means and the shift in radial scale D_r to their fiducial model they obtain for the BAO model $\chi^2 = 12.6$ ($k = 0$) as listed in Table 2, and for BAO+mag they obtain $\chi^2 = 9.7$ ($k = 1$). Comparing BAO to their $\xi = 0$ ($\chi^2 = 14$; $k = 0$) we obtain $\Delta\chi^2 = 1.4$, showing no significant improvement (slightly above 1σ). Comparing BAO+mag to $\xi = 0$ we obtain BIC=1.4 and AIC=2.4.

We also examine our Horizon Run model and $\xi = 0$ to their data. We use our DR7-Full co-

variance matrix, though normalize it by using the ratio of volumes of DR7 and DR6 (see caption in Table 2), and obtain $\Delta\chi^2 = 1.4$. We conclude that using the DR6 data the physical models do not out-perform $\xi = 0$ in a significant manner.

In the case of DR7-Full data we see that the fiducial Horizon Run model performs better than $\xi = 0$ ($\Delta\chi^2 = 3.1$). This does not yield much confidence that we have detected a line-of-sight peak for a few reasons. First, the model baryonic acoustic feature is much weaker than the strong clustering in the data (Figure 3). Second, the physical model is preferred by less than 2σ. Third, The number of bins might be of concern. We conduct tests with wider bins ($\Delta\pi \sim 10\,h^{-1}$Mpc), and obtain a better agreement between the models $\Delta\chi^2 = 1.1$. This shows that the criterion is sensitive to the width of the binning when $k = 0$.

We note that the $\xi = 0$ fit to DR7-Full is much worse than that to DR6 (GCH data). We mentioned the normalization of the C_{ij}; without this normalization we obtain only slightly better fits. Another notable difference that might contribute to this discrepancy is that that the GCH data is much smoother than ours. They explain binning techniques applied on the data, which we do not perform here. Another noticeable difference are the two bins centered around $112.5\,h^{-1}$Mpc and $117.5\,h^{-1}$Mpc. In GCH DR6 results they are positive and form a wide range of positive overdensity. In DR7 we show in Figure 3, as well as Figure 12 in GCH (see their red lines) that these two bins are negative.

We emphasize here that many assumptions are made when performing this comparison. We assume C_{ij} is model independent, but do not expect it to change significantly within parameter space. In addition, we assume the likelihood to be Gaussian and the correctness of the BIC and AIC. As noted above, we find sensitivity in $\Delta\chi^2$ model comparisons when varying size of π bins.

To summarize, both studies demonstrate that the line-of-sight measurement is very noisy (in a χ^2 sense). It is our opinion that these correlation functions do not convincingly show a line-of-sight feature.

The main distinctions between our conclusions and those of GCH, is that when investigating significance we take into account the addition of free parameters k, as well as the importance of the $\xi = 0$ test. k serves in both BIC and AIC as a "penalty" for adding parameters. Ignoring k (which is the wrong thing to do) would cause this test to favor a BAO model with magnification, where including it, this comparison shows that the current data can not distinguish between physical models in a convincing manner. The physical models do perform better than a No BAO model, This last point, however, is not proof for detection of a peak in the line-of-sight clustering. No BAO is not physically motivated, and there is no *physical* reason to prefer this model over other featureless models. We show here that the physical models do not perform better significantly than a null $\xi = 0$, which yields a good fit to the data.

The reader should keep in mind that there is no apparent correct answer to the issue at hand for the current data. In order to detect a significant line-of-sight baryonic acoustic feature, which can be used to determine $H(z)$ and ultimately the expansion rate of the nearby universe, noise must be reduced by probing larger volumes.

In the following section, we examine the line-of-sight signal expected in a much larger volume survey.

7. Prediction: BOSS Line-of-Sight Clustering

The Baryonic Oscillation Spectroscopic Survey (BOSS; Schlegel et al. 2009) plans to map 1.5 million LRGs in a much larger volume than DR7, up to $z \sim 0.7$. We examine here what can be expected from the line-of-sight correlation function in the BOSS volume.

Figure 4 displays the predictions for the line-of-sight signal. In this case we work in π-r_p space and define the line-of-sight using a cut at $r_p = 5.5\ h^{-1}$Mpc (using $\Delta\pi = 5\,h^{-1}$Mpc bins). The solid red line is the line-of-sight prediction for the mean BOSS signal, and the gray band is the 1σ sample variance. The black thick diamonds are

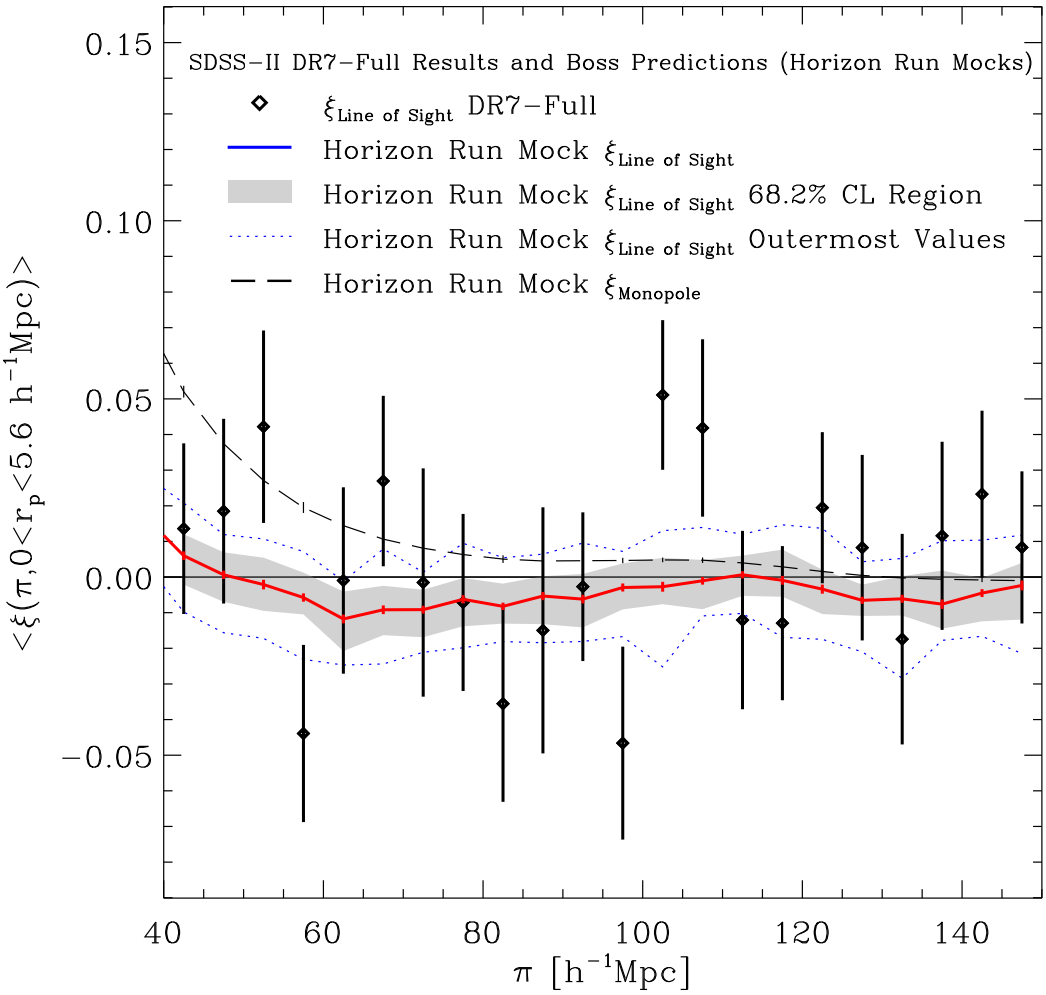

Fig. 4.— DR7-Full vs expected BOSS Line-of-sight $\xi(\pi, r_p < 5.5\,h^{-1}\mathrm{Mpc})$. The red line is the mean of the Horizon Run predictions for the BOSS volume. The 68.2% CL region is the gray band. The diamonds are the SDSS-II measurement from DR7-Full (same as in Figure 3) The apparent high clustering excess in the current data at $\pi \sim 110\,h^{-1}$Mpc should be excluded (or confirmed) at a high confidence level by the BOSS data. For comparison, the dashed line shows the mock monopole (with 1σ uncertainties for a given BOSS volume).

the observed results from DR7-Full using the same line-of-sight definition (same values as in Figure 3). The dashed line shows the expected monopole prediction for comparison.

Although the line-of-sight mock signal is negative at these scales due to the linear redshift-space distortions (the squashing effect), there is a signature of a peak with a position in fair agreement with the monopole. The 1σ uncertainties suggest, however, that even in BOSS we do not expect a significant line-of-sight detection of the baryonic acoustic feature, if we define the line-of-sight as narrowly as GCH do (that is, within $\theta < 3^\circ$ or $r_p < 5.5\,h^{-1}$Mpc).

The estimated uncertainties do indicate that BOSS will have the statistical power to rule out (or confirm) at high confidence a clustering excess at the level claimed by GCH at $\pi \sim 110\,h^{-1}$Mpc . To test this proposition quantitatively, we evaluate χ^2 of the DR7-Full result versus the model constructed from the Horizon Run mock mean, using all 32 realizations to determine the covariance matrix. We obtain $\chi^2 = 151$ for 4 degrees of freedom (the bins between $100 < \pi < 120\,h^{-1}$Mpc). Our mocks thus predict that a measurement as strong as that seen in DR7-Full is extremely unlikely in BOSS.

In Figure 5 we examine the uncertainties of the line-of-sight (left panels) and monopole (top right panel) measurements of the correlation function. We examine differences between the two line-of-sight definitions: the top left panel shows for $\theta < 3^\circ$, and the bottom $r_p < 5.5\,h^{-1}$Mpc. Included in this figure are the estimates of the DR7-Sub sample (both using LasDamas and using data jackknife subsamples), DR6 (as estimated by GCH), DR7-Full (Horizon Run) and for BOSS (Horizon Run). Finally, we also compare our monopole predictions to those found using the linear theory estimate of Cohn (2006). For descriptions of the mocks realizations used please refer to §2.2.

The top left panel of Figure 5 shows results for the line-of-sight ($\theta < 3^\circ$). For comparison, the solid line is the expected signal (in absolute value) using the BOSS mocks from the Horizon Run. The thick dashed line shows the uncertainty estimates for this case, demonstrating again that even in BOSS the line-of-sight signal, as defined here, will be very difficult to measure. The thin dashed line shows our error estimates using the LasDamas DR7-Sub mocks. For comparison the diamonds show jackknife estimates of the uncertainties from the data itself, which are in excellent agreement with the mocks. Obviously, the SDSS-II results are much noisier than the BOSS results will be.

The bottom panel shows the same predictions but when defining the line-of-sight region as $r_p < 5.5\,h^{-1}$Mpc. The medium width dashed red line corresponds to our DR7-Full uncertainties, the purple triangles are uncertainties according to GCH (see their Table 1). The DR7-Sub uncertainty (thin blue dashed line), the predicted BOSS signal (thick solid black line) and uncertainty (thick dashed black line) has the same notation as before. Cabré & Gaztañaga (2009) argue that at $\pi > 20\,h^{-1}$Mpc shot noise dominates the noise.

Comparing the BOSS results, we see clear differences between the uncertainties in the two coordinate systems. The $s - \theta$ has a negative slope in respect to scale where the $\pi - r_p$ has a very slight positive slope (also noticeable in Figure 3). The reason for this is simple: $\theta < 3^\circ$ corresponds to a cone, whereas $r_p < 5.5\,h^{-1}$Mpc corresponds to a cylinder. The uncertainties in the former decrease with s because more data is included, reducing the noise. The latter is very flat, because all scales each bin contains roughly the same number of pairs. The slight positive slope indicates minor effects of boundary conditions at these scales. We thank E. Gaztañaga for pointing this difference out in a private communication.

As a consistency check, we verified that, although the scale dependence differs, the uncertainty for BOSS at $\sim 100\,h^{-1}$Mpc is similar in the two coordinate systems, as expected.

Our DR7-Full uncertainties are in excellent agreement with those of GCH. This result is slightly surprising, because we expect our DR7-Full uncertainties to be slightly smaller than those obtained by GCH, who investigate the slightly

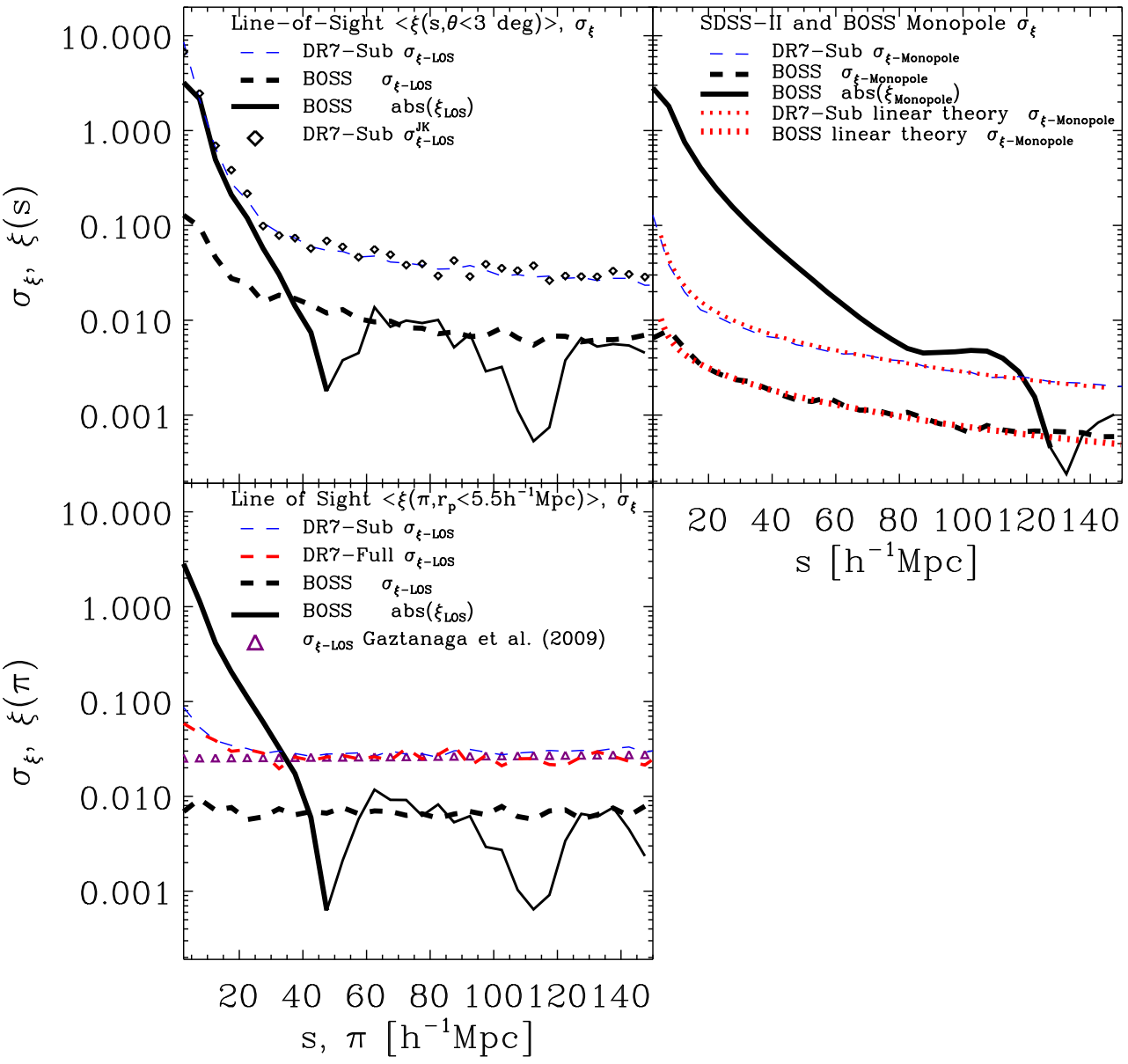

Fig. 5.— DR7-Sub, DR7-Full and BOSS line-of-sight and monopole ξ and uncertainties σ_ξ. Top left panel shows the line-of-sight (defined as $\Delta\theta < 3°$). The solid line is $|\xi_{\rm LOS}|$ (where thick is positive and thin negative values). The dashed lines are the line-of-sight uncertainties $\sigma_{\xi-{\rm LOS}}$ based on mock catalogs. The thin dashed line is for DR7-Sub (using LasDamas mocks), and the thick dashed line is for BOSS (using Horizon Run mocks). The diamonds show jackknife uncertainty estimates for DR7-Sub data. The bottom left panel is similar where line-of-sight is defined as $r_p < 5.5\,h^{-1}$Mpc. Differences- red dashed is DR7-Full results (using Horizon Run mocks), which agree very well with results from GCH (purple triangles). The right panel shows the same quantities as top left for the monopole. The solid line is $|\xi_{\rm Monopole}|$. The dashed lines are its uncertainties $\sigma_{\xi-{\rm Monopole}}$ based on mock catalogs. The thin dashed line is for DR7-Sub, and the thick dashed line is for BOSS. The dotted lines show the estimates from linear theory based on Cohn (2006). The thin dotted line is for DR7-Sub, and the thick dotted line is for BOSS.

smaller DR6 volume. This might be an artifact of the way we subsampled the Horizon Run mocks, as explained in §2.2. Overall, however, we consider our result to be in general agreement with those of GCH.

The right panel shows results for the monopole. For comparison, the solid line is the absolute value of the expected signal from the BOSS mocks. The thin dashed line shows the uncertainty estimates from LasDamas for SDSS-II (DR7-Sub). The thick dashed line shows the uncertainty estimates from Horizon Run for BOSS, which are obviously much smaller. The thin and thick dotted lines show the estimates for each survey from linear theory (Cohn 2006), which are in remarkable agreement with the mock catalog results. This comparison demonstrates that our estimates from the mock catalogs are reasonable and strengthens our confidence in our estimates for the line-of-sight error estimates.

BOSS will have a larger volume than DR7-Sub, and hence yields much smaller uncertainties in $\sigma_{\xi-\mathrm{LOS}}$ (line-of-sight) and $\sigma_{\xi-\mathrm{Monopole}}$ (monopole). We estimate that the monopole uncertainty at the baryonic acoustic feature will be reduced by a factor of four and the line-of-sight signal by approximately the same amount We predict the signal-to-noise for BOSS at the baryonic acoustic feature scale at $S/N \equiv |\xi_{\mathrm{Monopole}}|/\sigma \sim 6$. These calculations are based on a single bin, so should be considered a lower limit of the true statistical power of the survey.

Notice that the BOSS $\sigma_{\xi-\mathrm{LOS}}$ (left panel of Figure 5) is expected to be slightly larger than that of the SDSS-II $\sigma_{\xi-\mathrm{Monopole}}$ (right panel of Figure 5). Moreover, the BOSS ξ_{LOS}, appears negative at scales larger than $s > 50\,h^{-1}$Mpc, resulting in a baryonic acoustic dip in the left panel, which is significantly smaller in absolute magnitude than $\sigma_{\xi-\mathrm{LOS}}$, making a detection of the feature unlikely.

We emphasize that the low signal-to-noise we predict is a result of the very small angular range that GCH chose to study. Our results should not discourage us from disentangling D_{A} and H using the BOSS sample, as we describe in the next section.

8. Separating Line-of-Sight and Transverse Clustering in BOSS

As described above, the angle-averaged clustering (the monopole) constrains the combination $D_{\mathrm{A}}^2/H(z)$. The transverse signal probes $D_{\mathrm{A}}(z)$, which in turn is related to an integral of $H(z)$. This is limits the constraining power of $D_{\mathrm{A}}(z)$ due to degeneracies. The line-of-sight feature, however, constrains $H(z)$ directly at the mean sample redshift. Therefore, by measuring at the feature in various z slices, we can measure its change over time.

In previous sections we demonstrated that a narrow line-of-sight signal is not obtainable in the SDSS-II LRG sample, and should be noisy in BOSS.

A higher signal-to-noise ratio can be obtained in the data by using larger angular slices. In Figure 6 we follow the same procedure as before: this time with wider angular slices. The top right panel displays results for angular slices split at $\theta = 45°$. The solid red line is the line-of-sight result, now defined as $\langle\xi(s, 0° < \theta < 45°)\rangle$ and the dotted blue line is the transverse result $\xi(s, 45° < \theta < 90°)$. DR7-Full results are the symbols. The expected redshift-space signals are the thick lines; the gray bands are the 1σ uncertainties expected from one BOSS volume. For comparison, the expected monopole ($\langle\xi(s, 0° < \theta < 90°)\rangle$) is the dashed black line. The uncertainties in the transverse signal are smaller than the line-of-sight, because the former contains much more information than the latter (c.f. the $\sin(\theta)$ factor in Equation 2).

The clear vertical offset between the line-of-sight signal and the transverse signal is a result of redshift distortions. We note that in the resulting region where the correlation function is negative, there is a clear sign for a trough-peak-trough.

As a consistency check for our software, when analyzing the Horizon Run real-space catalog, we have verified that the offset in signal is not present; in real-space, both the line-of-sight and transverse correlation functions have a similar signal as the monopole, as expected.

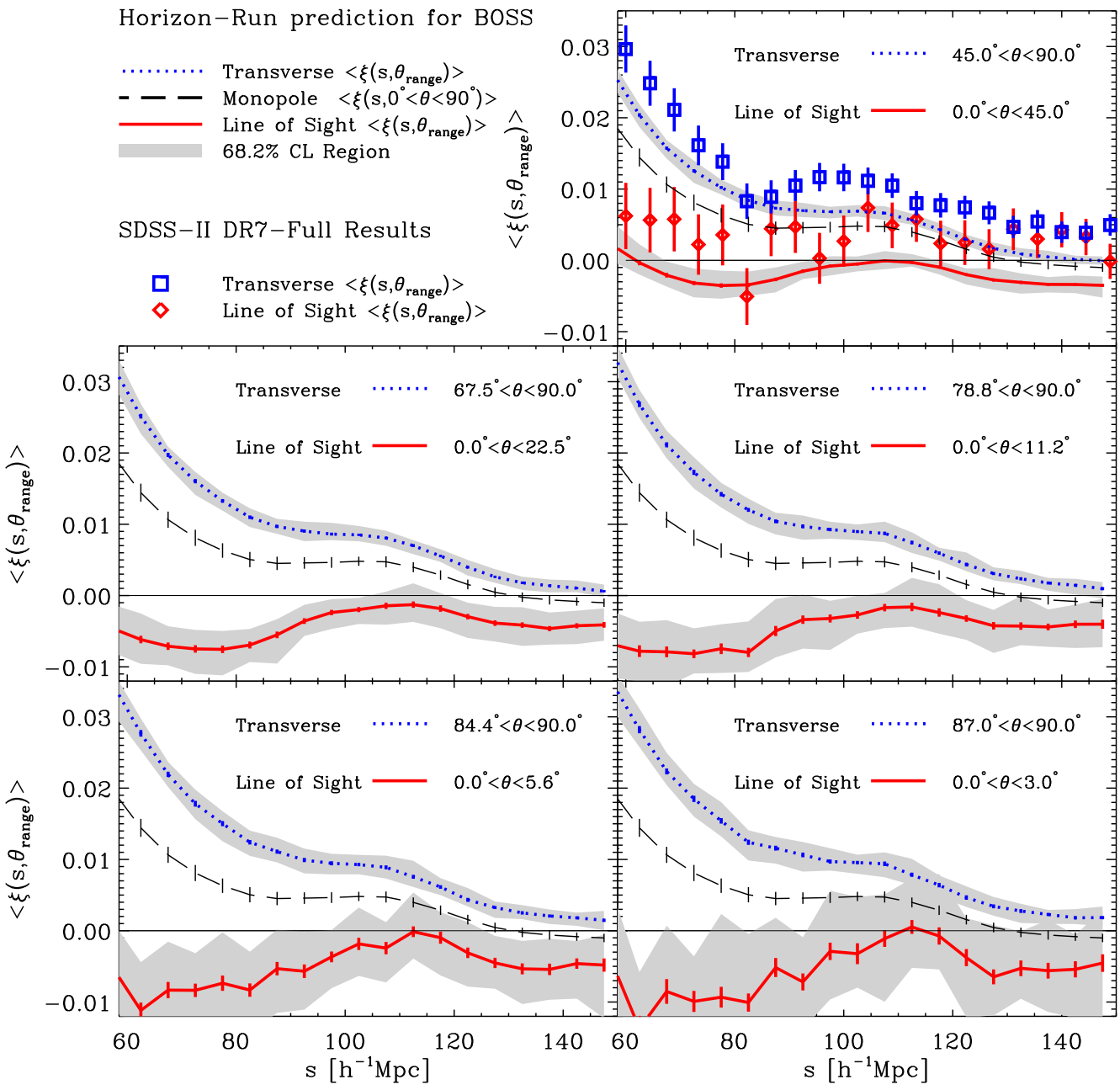

Fig. 6.— BOSS expected line-of-sight and transverse angular slices of ξ. Each panel shows two angular wedges of the redshift-space correlation function $\xi(s)$ as predicted for BOSS from the Horizon Run simulations. The size of the wedges are indicated in each panel (starting at 45° at the top and decreasing towards the bottom). The solid red lines show the wedges closest to the line-of-sight direction, and the dotted blue lines show the wedges closest to the tranverse direction. In each case we give the 1σ uncertainty in the mock mean as the error bars and the uncertainty for a single BOSS volume as the gray band. The angular slices are $\Delta\theta = 45°$, $22.5°$, $11.2°$, $5.6°$ and $3°$. The dashed line is the monopole prediction and is the same in all panels, with uncertainties given for one BOSS volume (i.e., not the mock mean). The symbols in the top right panel are the result for DR7-Full in the $\Delta\theta = 45°$ slices, where red diamonds are for the line-of-sight direction and the blue squares are for the transverse direction.

In the subsequent panels we slice the anisotropic ξ into finer angular divisions (each $\Delta\theta$ is indicated in the legend and the caption). Again for each wedge size, we display the wedges closest to the line-of-sight direction (solid red line), and closest to the transverse direction (dotted blue line). We plot the monopole result in each panel for comparison (black dashed line). Although the signal is noisier for smaller wedges, a clear detection of the relative peak position in each direction appears obtainable by BOSS.

We defer to the future a thorough analysis of the precision with which BOSS will measure $H(z)$ and $D_{\rm A}$ by measuring the baryonic acoustic feature as a function of angle θ. Here we simply note that the low signal-to-noise ratio expected for the very narrow line-of-sight cone studied by GCH should not discourage us from this measurement.

This independent measure of the line-of-sight and transverse features in clustering can be interpreted as a test of the Alcock & Paczynski (1979) effect. When counting pairs we have assumed a fiducial cosmology for the purpose of converting the observed redshifts to comoving distances. Although this cosmology is well motivated by WMAP 5-year results (Komatsu et al. 2009), small deviations from the true underlying cosmology will result in distortions in ξ, and of most concern, the position of the baryonic acoustic feature.

Alcock & Paczynski (1979) describe how an intrinsically spherical body in real-space appears distorted to an observer who measures the object in redshift-space and uses an incorrect cosmology to convert to comoving space. In real-space the baryonic acoustic feature appears as such a spherical body (in the statistical sense) and the line of sight baryonic acoustic feature should yield the same result as the transverse direction.

The spherical nature of the baryonic acoustic feature is only approximate in redshift-space because it is somewhat distorted due to gravitational dynamics. However, the effect of these dynamic distortions on the position of the feature are understood. Thus, by comparing the line-of-sight feature to the transverse feature, we can learn about the true underlying cosmology.

We emphasize that in Figure 6 we merely show disentanglement of line-of-sight and transverse clustering signals. We do not perform the Alcock & Paczynski (1979) test as the fiducial cosmology used to calculate mock ξ is the same as the simulations.

9. Discussion and Conclusions

In this paper we demonstrate that the claim of a *significant detection* in the line-of-sight baryonic acoustic feature in the SDSS LRG sample by GCH is unjustified. We perform a similar analysis to theirs, and obtain similar results. The main difference in our interpretation, as we elaborate in §6, is that we use a more conservative criterion regarding whether we detect a feature. We find that the data agrees very well with a ΛCDM redshift-space non-linear model tested here, which does not contain a clear line-of-sight feature due to its low signal-to-noise ratio. We also find that physical line-of-sight models tested by us and GCH do not out-perform a null $\xi = 0$ model, indicating no clear evidence of a line-of-sight baryonic acoustic feature. The BOSS survey, which has just begun, will have the statistical power to rule out (or confirm) this strong clustering excess at high significance (Figure 4), though not to usefully detect the baryonic acoustic feature in such a narrowly defined line-of-sight measurement. By using broader angular bins, BOSS will be able to independently measure baryonic acoustic feature along the line-of-sight and transverse directions.

We examine two different volumes in the SDSS LRG sample (SDSS-II). In the smaller one ($0.16 < z < 0.36$; DR7-Sub; §4), for which we use very realistic mock catalogs, we find a good agreement ($1\sigma - 1.5\sigma$) between the line-of-sight observation and a ΛCDM model, which does not have an apparent feature even in ~ 160 DR7-Sub volumes. For our full sample ($0.16 < z < 0.47$; DR7-Full) we find that a fiducial model agrees within $1.5\sigma - 2\sigma$.

Figures 2, 3, 5 clearly show that the line of sight clustering excess at $s \sim 110\,h^{-1}$Mpc in both volumes is dominated by noise.

We confirm the number of pairs estimate of

Miralda-Escude (2009) which they used on GCH results. The bin of interest is $106.7 < s < 111.1\,h^{-1}$Mpc and $0^\circ < \theta < 3^\circ$, corresponding to the choice in GCH of $\Delta\pi$ and $r_p < 5.5\,h^{-1}$Mpc. In our case, we count the number of effective pairs, including the effects of weighting (see Kazin et al. 2010 for details). DR7-Sub yields 2259 pairs and DR7-Full yields 3104. Examining 160 very realistic mock catalogs, we find that the high DR7-Sub value of $\xi = 0.085$ in this bin, although unlikely, is consistent with ΛCDM (one mock of 160 has a higher value).

We point out that the strong clustering excess that *happens to be at the correct scale* is *probably* noise, that will be reduced with increase of volume. We see a hint of this effect when the volume increases from DR7-Sub ($0.66\,h^{-3}$Gpc^3) to DR7-Full ($1.6\,h^{-3}$Gpc^3) the line-of-sight clustering excess ($\theta < 3^\circ$) at $s \sim 108.9\,h^{-1}$Mpc is decreased from $\xi \sim 0.085$ to $\xi \sim 0.045$. This is shown also in GCH in their Figures 13 and 15. We interpret the difference between both measurements and the expected value from ΛCDM as noise.

Assuming correctness of our fiducial cosmology, the predicted BOSS results, presented in Figure 4, show that the strong line-of-sight clustering excess seen in DR7 should be ruled out at a very high confidence level when measuring ξ in the BOSS LRG sample.

In the left panels of Figure 5 we show the low S/N expected from the line-of-sight measurement in BOSS. We also examine by eye all 32 line-of-sight results (defined as $r_p < 5.5\,h^{-1}$Mpc), and find that 7 of 32 ($\sim 22\%$) mocks do not show a clear line-of-sight baryonic acoustic feature, where 12 do show a clear signal ($\sim 38\%$). This analysis is, of course, subjective, but suggests that the LRGs alone, might not detect the line-of-sight baryonic acoustic feature in the BOSS volume, if the line-of-sight definition is limited to $\theta < 3^\circ$ or $r_p < 5.5\,h^{-1}$Mpc.

In Figure 6 we show, however, reason for optimism in disentangling $H(z)$ and $D_{\rm A}(z)$ in the future BOSS LRG data. Unsurprisingly, using wider angular cuts yields better signal-to-noise ratio results. The various $\Delta\theta$ slices contain line-of-sight and transverse information that may be used to probe $H(z)$ and $D_{\rm A}(z)$.

Throughout this study, we have ignored the effects of any potential reconstruction techniques that might be employed on the BOSS data (Eisenstein et al. 2007, Huff et al. 2007, Padmanabhan et al. 2009, Noh et al. 2009). Reconstruction may allow better precision in measuring the peak position than indicated here.

We emphasize that our measurements and uncertainty estimates are similar to those carried out previously by GCH. We also confirm that the strong clustering signal at the line-of-sight can not be explained by systematics. We check various binning widths in both π and r_p as well as fiber-collision weightings, and do not find significant changes. We do, however, disagree on interpretation of the results.

The main dispute is regarding the use of the strong line-of-sight clustering in the data as the baryonic acoustic feature to determine H(z) directly. In their Table 3 GCH show results for $H(z)$ obtained by two different methods:

1. "Shape Method": using the full shape of the line-of-sight clustering with priors from monopole, quadrupole clustering as well as CMB temperature fluctuations to determine $H(z)/H_0$.

2. "Peak Method": using the line-of-sight baryonic acoustic feature peak position to determine $H(z)$ directly.

While both methods are correct procedures to perform, the second should be considered valid only if the line-of-sight baryonic acoustic feature is convincingly detected.

To explain the insignificance of a detection, we consider the null $\xi = 0$ test. Using a Jeffreys scale, in §6 we show that the physical models do not outperform $\xi = 0$. This does not mean, of course, that $\xi = 0$ is the line-of-sight clustering at these scales, but rather indicates that models can not be distinguished significantly and a clear line-of-sight baryonic acoustic feature can not be declared detected using this data set.

Only future surveys can show definitively what the line-of-sight correlation function is in these bins. In particular, BOSS will be able to do so. In Figure 4 we show that BOSS, which is underway, will be able to rule out this detection or verify it. BOSS is due to cover a comoving volume of ($\sim 8.1\,h^{-3}\mathrm{Gpc}^3$; $0.16 < z < 0.80$) by 2014. For a comoving volume of $\sim 3.9\,h^{-3}\mathrm{Gpc}^3(0.16 < z < 0.60)$ and density expected in BOSS, we find that all our 32 mock realizations have an apparent *monopole* feature (as opposed to SDSS-II volumes, Kazin et al. 2010).

Another survey that is on its way to refine baryonic acoustic feature measurements is the WiggleZ. The WiggleZ Dark Energy Survey (Drinkwater et al. 2010) is expected to complete very soon a narrower redshift survey (area $\sim 1,000$ deg^2), using Blue Emission Line Galaxies, in a comoving volume of $\sim 1\mathrm{Gpc}^3$ between $0.2 < z < 1$. When analyzing a quarter of the predicted final sample, Blake et al. (2010) show in Figure 20 a hint of a baryonic acoustic wiggle in the P(k) monopole. Although it is not clear whether this survey will detect a significant peak in the line-of-sight ξ (assuming $\theta < 3^\circ$), we are hopeful it will give us indication of the true signal.

If the claim for detection by GCH is correct, the unexpected strong line-of-sight signal would require an explanation.

It is a pleasure to thank Enrique Gaztañaga for commenting in detail on our draft, in depth discussions on interpretation, uncertainty estimation issues and sharing information regarding analysis. We thank Lam Hui and David Hogg for discussing interpretation of results, as well as Anna Cabre who shared with us her results. We thank Nic Ross for his very useful comments which helped clarify our draft. We thank Daniel Eisenstein for assistance in selecting LRGs and Idit Zehavi for discussions on weighting algorithms and selection function considerations. We thank Nikhil Padmanabhan, Nic Ross and David Schlegel for BOSS related discussions. We also thank Vincent Desjacques, Abraham Loeb, Ariel Sánchez, and Martin White for useful discussions and insight. We thank the LasDamas collaboration (http://lss.phy.vanderbilt.edu/lasdamas/) for making their mock catalogs publicly available. Thanks are also due to the Horizon team (http://astro.kias.re.kr/Horizon-Run/) for making their mocks public, and in particular Changbom Park and Juhan Kim for discussions on usage. E.K thanks Jo Bovy and Mulin Ding for their technical help. E.K thanks David Schlegel and Nic Ross at Lawrence Berkeley National Lab for their hospitality during part of the analysis in March. E.K was partially supported by a Google Research Award and NASA Award NNX09AC85G. M.B was supported by Spitzer G05-AR-50443 and NASA Award NNX09AC85G. R.S. was partially supported by NSF AST-0607747 and NASA NNG06GH21G.

Funding for the SDSS and SDSS-II has been provided by the Alfred P. Sloan Foundation, the Participating Institutions, the National Science Foundation, the U.S. Department of Energy, the National Aeronautics and Space Administration, the Japanese Monbukagakusho, the Max Planck Society, and the Higher Education Funding Council for England. The SDSS Web Site is http://www.sdss.org/.

The SDSS is managed by the Astrophysical Research Consortium for the Participating Institutions. The Participating Institutions are the American Museum of Natural History, Astrophysical Institute Potsdam, University of Basel, University of Cambridge, Case Western Reserve University, University of Chicago, Drexel University, Fermilab, the Institute for Advanced Study, the Japan Participation Group, Johns Hopkins University, the Joint Institute for Nuclear Astrophysics, the Kavli Institute for Particle Astrophysics and Cosmology, the Korean Scientist Group, the Chinese Academy of Sciences (LAMOST), Los Alamos National Laboratory, the Max-Planck-Institute for Astronomy (MPIA), the Max-Planck-Institute for Astrophysics (MPA), New Mexico State University, Ohio State University, University of Pittsburgh, University of Portsmouth, Princeton University, the United States Naval Observatory, and the University of Washington.

REFERENCES

Abazajian, K. et al. 2009, ApJS, to appear, (arXiv:0812.0649)

Adelman-McCarthy, J. K., Agüeros, M. A., Allam, S. S., Prieto, C. A., Anderson, K. S. J., Anderson, S. F., Annis, J., Bahcall, N. A., Bailer-Jones, C. A. L., Baldry, I. K., Barentine, J. C., Bassett, B. A., Becker, A. C., Beers, T. C., Bell, E. F., Berlind, A. A., Bernardi, M., Blanton, M. R., Bochanski, J. J., Boroski, W. N., Brinchmann, J., Brinkmann, J., Brunner, R. J., Budavári, T., Carliles, S., Carr, M. A., Castander, F. J., Cinabro, D., Cool, R. J., Covey, K. R., Csabai, I., Cunha, C. E., Davenport, J. R. A., Dilday, B., Doi, M., Eisenstein, D. J., Evans, M. L., Fan, X., Finkbeiner, D. P., Friedman, S. D., Frieman, J. A., Fukugita, M., Gänsicke, B. T., Gates, E., Gillespie, B., Glazebrook, K., Gray, J., Grebel, E. K., Gunn, J. E., Gurbani, V. K., Hall, P. B., Harding, P., Harvanek, M., Hawley, S. L., Hayes, J., Heckman, T. M., Hendry, J. S., Hindsley, R. B., Hirata, C. M., Hogan, C. J., Hogg, D. W., Hyde, J. B., Ichikawa, S.-I., Ivezić, Ž., Jester, S., Johnson, J. A., Jorgensen, A. M., Jurić, M., Kent, S. M., Kessler, R., Kleinman, S. J., Knapp, G. R., Kron, R. G., Krzesinski, J., Kuropatkin, N., Lamb, D. Q., Lampeitl, H., Lebedeva, S., Lee, Y. S., Leger, R. F., Lépine, S., Lima, M., Lin, H., Long, D. C., Loomis, C. P., Loveday, J., Lupton, R. H., Malanushenko, O., Malanushenko, V., Mandelbaum, R., Margon, B., Marriner, J. P., Martínez-Delgado, D., Matsubara, T., McGehee, P. M., McKay, T. A., Meiksin, A., Morrison, H. L., Munn, J. A., Nakajima, R., Neilsen, E. H., Newberg, H. J., Nichol, R. C., Nicinski, T., Nieto-Santisteban, M., Nitta, A., Okamura, S., Owen, R., Oyaizu, H., Padmanabhan, N., Pan, K., Park, C., Peoples, J., Pier, J. R., Pope, A. C., Purger, N., Raddick, M. J., Fiorentin, P. R., Richards, G. T., Richmond, M. W., Riess, A. G., Rix, H.-W., Rockosi, C. M., Sako, M., Schlegel, D. J., Schneider, D. P., Schreiber, M. R., Schwope, A. D., Seljak, U., Sesar, B., Sheldon, E., Shimasaku, K., Sivarani, T., Smith, J. A., Snedden, S. A., Steinmetz, M., Strauss, M. A., SubbaRao, M., Suto, Y., Szalay, A. S., Szapudi, I., Szkody, P., Tegmark, M., Thakar, A. R., Tremonti, C. A., Tucker, D. L., Uomoto, A., Berk, D. E. V., Vandenberg, J., Vidrih, S., Vogeley, M. S., Voges, W., Vogt, N. P., Wadadekar, Y., Weinberg, D. H., West, A. A., White, S. D. M., Wilhite, B. C., Yanny, B., Yocum, D. R., York, D. G., Zehavi, I., & Zucker, D. B. 2008, The Astrophysical Journal Supplement Series, 175, 297, (c) 2008: The American Astronomical Society

Akaike, H. 1974, The Annals of Statistics, 19, 461

Alcock, C. & Paczynski, B. 1979, Nature, 281, 358

Berlind, A. A. & Weinberg, D. H. 2002, ApJ, 575, 587

Blake, C., Brough, S., Colless, M., Couch, W., Croom, S., Davis, T., Drinkwater, M. J., Forster, K., Glazebrook, K., Jelliffe, B., Jurek, R. J., Li, I., Madore, B., Martin, C., Pimbblet, K., Poole, G. B., Pracy, M., Sharp, R., Wisnioski, E., Woods, D., & Wyder, T. 2010, ArXiv e-prints

Blake, C., Collister, A., Bridle, S., & Lahav, O. 2007, MNRAS, 374, 1527

Blake, C. & Glazebrook, K. 2003, ApJ, 594, 665

Cabré, A. & Gaztañaga, E. 2009, MNRAS, 393, 1183

Cohn, J. D. 2006, New Astronomy, 11, 226

Cole, S., Percival, W. J., Peacock, J. A., Norberg, P., Baugh, C. M., Frenk, C. S., Baldry, I., Bland-Hawthorn, J., Bridges, T., Cannon, R., Colless, M., Collins, C., Couch, W., Cross, N. J. G., Dalton, G., Eke, V. R., De Propris, R., Driver, S. P., Efstathiou, G., Ellis, R. S., Glazebrook, K., Jackson, C., Jenkins, A., Lahav, O., Lewis, I., Lumsden, S., Maddox, S., Madgwick, D., Peterson, B. A., Sutherland, W., & Taylor, K. 2005, MNRAS, 362, 505

Colless, M., Peterson, B. A., Jackson, C., Peacock, J. A., Cole, S., Norberg, P., Baldry, I. K., Baugh, C. M., Bland-Hawthorn, J., Bridges, T., Cannon, R., Collins, C., Couch, W., Cross, N., Dalton, G., De Propris, R., Driver, S. P., Efstathiou, G., Ellis, R. S., Frenk, C. S., Glazebrook, K., Lahav, O., Lewis, I., Lumsden, S., Maddox, S., Madgwick, D., Sutherland, W., & Taylor, K. 2003, ArXiv Astrophysics e-prints

Drinkwater, M. J., Jurek, R. J., Blake, C., Woods, D., Pimbblet, K. A., Glazebrook, K., Sharp, R., Pracy, M. B., Brough, S., Colless, M., Couch, W. J., Croom, S. M., Davis, T. M., Forbes, D., Forster, K., Gilbank, D. G., Gladders, M., Jelliffe, B., Jones, N., Li, I., Madore, B., Martin, D. C., Poole, G. B., Small, T., Wisnioski, E., Wyder, T., & Yee, H. K. C. 2010, MNRAS, 401, 1429

Eisenstein, D. J., Seo, H.-J., Sirko, E., & Spergel, D. N. 2007, ApJ, 664, 675

Eisenstein, D. J. et al. 2005, ApJ, 633, 560

Gaztañaga, E., Cabré, A., & Hui, L. 2009, MNRAS, 399, 1663

Glazebrook, K. & Blake, C. 2005, ApJ, 631, 1

Hu, W. & Haiman, Z. 2003, Phys. Rev. D, 68, 063004

Hubble, E. & Humason, M. L. 1931, ApJ, 74, 43

Huff, E., Schulz, A. E., White, M., Schlegel, D. J., & Warren, M. S. 2007, Astroparticle Physics, 26, 351

Hui, L., Gaztañaga, E., & Loverde, M. 2007, Phys. Rev. D, 76, 103502

Hütsi, G. 2006, A&A, 449, 891

Jackson, J. C. 1972, MNRAS, 156, 1P

Kaiser, N. 1987, MNRAS, 227, 1

Kazin, E. A., Blanton, M. R., Scoccimarro, R., McBride, C. K., Berlind, A. A., Bahcall, N. A., Brinkmann, J., Czarapata, P., Frieman, J. A., Kent, S. M., Schneider, D. P., & Szalay, A. S. 2010, ApJ, 710, 1444

Kim, J., Park, C., Gott, J. R., & Dubinski, J. 2009, ApJ, 701, 1547

Komatsu, E., Dunkley, J., Nolta, M. R., Bennett, C. L., Gold, B., Hinshaw, G., Jarosik, N., Larson, D., Limon, M., Page, L., Spergel, D. N., Halpern, M., Hill, R. S., Kogut, A., Meyer, S. S., Tucker, G. S., Weiland, J. L., Wollack, E., & Wright, E. L. 2009, The Astrophysical Journal Supplement, 180, 330

Labini, F. S., Vasilyev, N. L., & Baryshev. 2009, ArXiv e-prints

Landy, S. D. & Szalay, A. S. 1993, ApJ, 412, 64

Liddle, A. R. 2009, Annual Review of Nuclear and Particle Science, 59, 95

Linder, E. V. 2003, Phys. Rev. D, 68, 083504

Martinez, V. J., Arnalte-Mur, P., Saar, E., de la Cruz, P., Pons-Borderia, M. J., Paredes, S., Fernandez-Soto, A., & Tempel, E. 2008, ArXiv e-prints

Matsubara, T. 2004, ApJ, 615, 573

Miralda-Escude, J. 2009, ArXiv e-prints

Noh, Y., White, M., & Padmanabhan, N. 2009, Phys. Rev. D, 80, 123501

Okumura, T., Matsubara, T., Eisenstein, D. J., Kayo, I., Hikage, C., Szalay, A. S., & Schneider, D. P. 2008, ApJ, 676, 889

Padmanabhan, N., White, M., & Cohn, J. D. 2009, Physical Review D, 79, 63523, (c) 2009: The American Physical Society

Padmanabhan, N. et al. 2007, MNRAS, 378, 852

Park, C. & Kim, J. 2007, in Revista Mexicana de Astronomia y Astrofisica Conference Series, Vol. 28, Revista Mexicana de Astronomia y Astrofisica Conference Series, ed. S. Kurtz, 93–102

Peebles, P. J. E. & Yu, J. T. 1970, ApJ, 162, 815

Percival, W. J., Cole, S., Eisenstein, D. J., Nichol, R. C., Peacock, J. A., Pope, A. C., & Szalay, A. S. 2007, Monthly Notices of the Royal Astronomical Society, 381, 1053

Percival, W. J., Reid, B. A., Eisenstein, D. J., Bahcall, N. A., Budavari, T., Fukugita, M., Gunn, J. E., Ivezic, Z., Knapp, G. R., Kron, R. G., Loveday, J., Lupton, R. H., McKay, T. A., Meiksin, A., Nichol, R. C., Pope, A. C., Schlegel, D. J., Schneider, D. P., Spergel, D. N., Stoughton, C., Strauss, M. A., Szalay, A. S., Tegmark, M., Weinberg, D. H., York, D. G., & Zehavi, I. 2009, ArXiv e-prints

Reid, B. A., Percival, W. J., Eisenstein, D. J., Verde, L., Spergel, D. N., Skibba, R. A., Bahcall, N. A., Budavari, T., Fukugita, M., Gott, J. R., Gunn, J. E., Ivezic, Z., Knapp, G. R., Kron, R. G., Lupton, R. H., McKay, T. A., Meiksin, A., Nichol, R. C., Pope, A. C., Schlegel, D. J., Schneider, D. P., Strauss, M. A., Stoughton, C., Szalay, A. S., Tegmark, M., Weinberg, D. H., York, D. G., & Zehavi, I. 2009, ArXiv e-prints

Sanchez, A. G., Crocce, M., Cabre, A., Baugh, C. M., & Gaztanaga, E. 2009, ArXiv e-prints

Schlegel, D., White, M., & Eisenstein, D. 2009, ArXiv e-prints

Schwarz, G. 1978, The Annals of Statistics, 6, 461

Seo, H.-J. & Eisenstein, D. J. 2003, ApJ, 598, 720

Tegmark, M. et al. 2006, Phys. Rev. D, 74, 123507

Turner, E. L., Ostriker, J. P., & Gott, III, J. R. 1984, ApJ, 284, 1

Yoo, J. & Miralda-Escudé, J. 2009, ArXiv e-prints

York, D. G. et al. 2000, AJ, 120, 1579

Zehavi, I., Eisenstein, D. J., Nichol, R. C., Blanton, M. R., Hogg, D. W., Brinkmann, J., Loveday, J., Meiksin, A., Schneider, D. P., & Tegmark, M. 2005, ApJ, 621, 22

This 2-column preprint was prepared with the AAS LaTeX macros v5.2.

TABLE 1
SDSS-II AND BOSS LRG SAMPLES

Sample	# of LRGs	$z_{\rm min}$	$z_{\rm max}$	$\langle z \rangle$	$M_{g,\rm min}$	$M_{g,\rm max}$	$\langle M_g \rangle$	Area ($\rm deg^2$)	Volume (h^{-3} Gpc^3)	Density (10^{-5} h^3 Mpc^{-3})
DR7-Sub	61,899	0.16	0.36	0.278	−23.2	−21.2	−21.65	7,189	0.66	9.4
DR7-Full	105,831	0.16	0.47	0.324	−23.2	−21.2	−21.72	7,908	1.58	6.7
BOSS[a]	1,200,000	0.16	0.60	0.444	–	–	–	10,000	3.89	30.8

[a]For BOSS we present estimates for $0.16 < z < 0.6$. The survey intends to observe $z < 0.8$ ($8.1\,h^{-3}$Gpc^3) but the comoving number density is expected to fall sharply at $z > 0.6$

TABLE 2
JEFFREYS SCALE TEST FOR LINE-OF-SIGHT MODELS

Data	Model	χ^2	k	N	$\chi^2/(N-k)$	$Prob$[%][c]	$-\ln E \sim \chi^2 + kln(N)$	$-\ln E \sim \chi^2 + 2k$
GCH DR6 ($0.15 < z < 0.30$)	No BAO	25	5	20	1.7	5	40.0	35.0
GCH DR6 ($0.15 < z < 0.30$)	BAO	21	5	20	1.4	13	36.0	31.0
GCH DR6 ($0.15 < z < 0.30$)	BAO+mag	15	6	20	1.1	38	33.0	27.0
GCH DR6 ($0.15 < z < 0.47$)	No BAO	18	5	20	1.2	26	33.0	28.0
GCH DR6 ($0.15 < z < 0.47$)	BAO	12	5	20	0.8	68	27.0	22.0
GCH DR6 ($0.15 < z < 0.47$)	BAO+mag	8	6	20	0.6	89	26.0	20.0
GCH DR6 ($0.15 < z < 0.47$)	$\xi = 0$	14	0	20	0.7	83	14.0	14.0
GCH DR6 ($0.15 < z < 0.47$)	BAO	12.6	0	20	0.6	89	12.6	12.6
GCH DR6 ($0.15 < z < 0.47$)	BAO+mag	9.7	1	20	0.5	96	12.7	11.7
GCH DR6 ($0.15 < z < 0.47$)[d]	$\xi = 0$	15.8	0	20	0.8	73	15.8	15.8
GCH DR6 ($0.15 < z < 0.47$)[d]	Horizon Run	17.2	0	20	0.9	64	17.2	17.2
DR7-Sub ($0.16 < z < 0.36$)	$\xi = 0$	23.2	0	20	1.2	28	23.2	23.2
DR7-Sub ($0.16 < z < 0.36$)	LasDamas	24.8	0	20	1.2	21	24.8	24.8
DR7-Full ($0.16 < z < 0.47$)[b]	$\xi = 0$	31.8	0	20	1.6	4.5	31.8	31.8
DR7-Full ($0.16 < z < 0.47$)[b]	Horizon Run	28.7	0	20	1.4	9.4	28.7	28.7
DR7-Full ($0.16 < z < 0.47$)[b]	$\xi = 0$	13.7	0	10	1.4	19	13.7	13.7
DR7-Full ($0.16 < z < 0.47$)[b]	Horizon Run	12.6	0	10	1.3	25	12.6	12.6

[b]For DR7-Full we use the C_{ij} based on 160 DR7-Sub mocks normalized by the C_{ii} of 32 DR7-Full mocks

[c]Assuming a χ^2 distribution this answers: What is the probability to obtain a random variable from a χ^2 distribution larger than in the χ^2 column?

[d]Here we apply our own DR7-Full C_{ij}[b] to the DR6 data in Table 1 of GCH. To the C_{ij} we also apply a normalization of the ratio of volumes of DR7 and DR6, 1.58/1.35, which takes into account different sky coverage as well as the fact that GCH use LRGs at $z > 0.15$.

NOTE.—$\xi_{\rm Line-of-Sight}$ Model Statistics: Models are as mentioned in text. The $\xi = 0$, although not physical, gives indication of how noisy the data is. The χ^2 is a statistic that tests how well each model fits the data. To compare goodness of two models calculate $\Delta \ln E$ (we present both BIC and AIC values). Following Table 1 from Liddle (2009): $\Delta \ln E < 1$ "Not worth more than a bare mention", $1 < \Delta \ln E < 2.5$ "Significant", $2.5 < \Delta \ln E < 5$ "Strong to very strong", $5 < \Delta \ln E$ "Decisive". For descriptions of LasDamas and Horizon Run mocks, please refer to §2.2. All tests are conducted on bins in the range $\pi = [40, 140]\, h^{-1}$Mpc.